# Room Temperature Atomic Layer Deposition of Elemental Antimony

Majeda Al Hareri, David J. H. Emslie*

Department of Chemistry, McMaster University, 1280 Main St W, Hamilton, ON, Canada, L8S 4M1.

**ABSTRACT:** Atomic layer deposition (ALD) of elemental antimony was achieved on hydrogen-terminated silicon (H-Si) and $SiO_2$/Si substrates using $Sb(SiMe_3)_3$ and $SbCl_3$ in the temperature range 23-65 °C. The mirror-like films were confirmed to be composed of crystalline antimony by XPS (for the film deposited at 35 °C) and XRD, with low impurity levels and strong preferential orientation of crystal growth relative to the substrate surface. To the best of our knowledge, this is the first example of room temperature thermal ALD (with demonstrated self-limiting growth) of a pure element. Film growth at 35 °C exhibited a substrate-enhanced mechanism, characterized by faster film growth for the first ~125 ALD cycles, where substantial deposition is occurring on the original substrate surface (GPC = 1.3 Å/cycle on $SiO_2$/Si, and 1.0 Å/cycle on H-Si), and slower film growth (GPC = 0.40 Å/cycle on $SiO_2$/Si, and 0.27 Å/cycle on H-Si) after ~125 cycles, once much of the initial substrate surface has been covered. Films deposited using 500-2000 ALD cycles were shown to be continuous by SEM. The use of less than 250 cycles afforded discontinuous films. However, in this initial growth phase, when deposition is occurring primarily on the original substrate surface, in-situ surface pre-treatment by $Sb(SiMe_3)_3$ or $SbCl_3$ (50 x 0.4 or 0.8 s pulses), followed by the use of longer precursor pulses (0.4 or 0.8 s) during the first 50 ALD cycles resulted in improved nucleation. For example, on H-Si, a continuous 6.7 nm thick film was produced after initial pre-treatment with 50 x 0.8 s pulses of $SbCl_3$, followed by 50 ALD cycles using 0.8 s pulses. The use of longer ALD pulses in the first 50 ALD cycles following surface pre-treatment is likely required in order to achieve complete reactivity with an increased density of reactive surface sites.

## INTRODUCTION

Atomic layer deposition (ALD) is a thin film deposition technique which relies upon self-limiting surface-based reactions between two different precursors. These precursors are delivered sequentially to the substrate surface in the vapour phase, with precursor pulses separated by inert gas purge steps to preclude gas-phase reactivity. Thermal ALD utilizes stable precursor molecules (unlike plasma-enhanced ALD which utilizes a stable precursor in combination with plasma-generated radicals); from herein ALD is used to refer to thermal ALD. A primary advantage of ALD is that it can provide access to thin films with enhanced uniformity and conformality relative to other deposition methods, especially on high aspect-ratio substrates. ALD methods have been reported for a range of materials,[1] including pure elements. Most of element ALD research has focused on the transition metals,[2-4] although ALD of main group elements such as Al,[5] Sn,[6] Sb[7] and Te[8] has also been described. Antimony ALD was achieved using $Sb(SiEt_3)_3$ and $SbCl_3$; film growth was observed at 95-250 °C, and self-limiting growth was demonstrated at 95 °C.[7]

Thin films of elemental antimony have recently seen a flurry of interest[9-13] in the context of phase change memory (PCM), where data storage is achieved by switching between crystalline and amorphous states.[14-16] The use of elemental antimony as a monoatomic PCM material was made possible by confinement of a 3-10 nm thick antimony film between oxide or nitride layers. Use of a pure element for PCM avoids problems with more complex PCM materials, such as deviations from ideal stoichiometry, which can be introduced during film deposition, or can occur as a result of compositional partitioning under operating conditions. The programmable optical nonlinearity of thin antimony films has also been investigated, demonstrating high potential for applications in nanophotonics and optoelectronics.[17]

Additionally, ultra-thin films of Sb could potentially find application for in-situ *n*-doping of semiconductor materials such as silicon. In recent years, monolayer doping (MLD) has been developed as a method for doping of silicon or germanium with group 15 (or group 13) elements.[18-23] This method involves surface functionalization with a monolayer of a dopant-containing molecule, followed by application of a capping layer such as $SiO_2$ (to minimize loss of dopant atoms to the surroundings during the next step), rapid thermal annealing to cause diffusion of the chemisorbed dopant atoms into the semiconductor material, and removal of the capping layer. MLD can enable ultra-shallow doping, and doping of 3-D structures without crystal damage. However, several drawbacks of MLD have been noted, including: (a) almost all of the molecules used for monolayer formation contain carbon, leading to inevitable carbon incorporation into the semiconductor, in some cases significantly deactivating the electrical activity of the dopant atoms,[19,20,24] (b) dopant concentrations higher than those provided by a monolayer of dopant-containing molecules are not readily achieved,[18,25] and (c) monolayer formation typically requires prolonged reaction with the dopant-containing molecule (liquid, or in solution) at elevated temperature.[20] ALD-fabricated ultra-thin films of group 15 elements could potentially circumvent these issues, providing (via thermal annealing) access to films with high dopant concentrations and minimal carbon contamination.

Herein we report thermal ALD of antimony on H-Si (hydrogen-terminated silicon) and $SiO_2$/Si (Si(100) with a layer of oxide) substrates at 23-65 °C using the precursors $Sb(SiMe_3)_3$ and $SbCl_3$. This precursor combination also resulted in improved nucleation on H-Si (at 35 °C), relative to the previously reported higher temperature Sb ALD method {$Sb(SiEt_3)_3$/$SbCl_3$ at 95 °C}. Thermal ALD processes capable of operation at room temperature are scarce, given that it requires: (a) precursors which are volatile enough to allow room temperature delivery, (b) precursors with sufficient reactivity to enable rapid surface-based reactivity during each ALD cycle, and (c) ALD reaction byproducts which are volatile enough to be efficiently removed from the substrate surface. Most other materials to have been deposited by room temperature thermal ALD are metal oxides (e.g. $Al_2O_3$,[26,27] $B_2O_3$,[28,29] ZnO,[26] $SiO_2$[30,31] and $TiO_2$[26]), with deposition utilizing $H_2O$ (or rarely $O_3$)[27] as the co-reactant. To the best of our knowledge, a pure element has not previously been deposited by thermal ALD (with demonstrated self-limiting growth) at room temperature.[32-35] Room temperature ALD processes are of particular interest as a means to enable deposition on thermally-sensitive substrates,[27] to minimize problems with agglomeration of low-melting films (e.g. Cu),[36] and to enable ALD using less complex (and less expensive) ALD reactors. Room temperature thermal ALD methods can also be beneficial for high-throughput roll-to-roll ALD techniques,[27] and for area-selective ALD using small molecule inhibitors,[37] where inhibitor desorption and undesired reactivity can be minimized at low temperature.

We also describe the use of in-situ surface (H-Si or $SiO_2$/Si) pre-treatment with $Sb(SiMe_3)_3$ or $SbCl_3$ as a method to improve nucleation during the initial growth phase of ALD. Deposition in ALD is highly dependent on the chemical nature of the surface, and surface pre-treatment has previously been reported as a means to improve nucleation, or to improve selectivity in area-selective ALD (AS-ALD),[37,38] either by promoting or inhibiting growth on a particular material. For example, $AlMe_3$, $AlMe_2Cl$ or $ZnEt_2$ pre-treatment has been used to enhance nucleation during Pt ALD (using $^{Me}CpPtMe_3$ with $O_2$ or $O_2$ plasma) on oxide surfaces such as $SiO_2$,[39-41] and $AlMe_3$ pre-treatment has been shown to enhance nucleation during Ru ALD (using $RuO_4$ and $H_2$) on $SiO_2$.[42] Conversely, pre-treatment with $Me_2Si(NMe_2)_2$ has been used to preferentially inhibit ALD growth of Ru (and to a lesser extent Pt) on $SiO_2$ while still permitting growth on H-Si or $MoS_2$,[43] and dodecanethiol pre-treatment has been used to inhibit ALD on copper, while allowing ALD on $SiO_2$ and TaN.[44]

## RESULTS AND DISCUSSION

Trialkylchlorosilane elimination reactivity between $Sb(SiMe_3)_3$ and $SbCl_3$ was investigated as a means to achieve room temperature thermal ALD of elemental antimony. This reactivity mirrors that previously reported by Pore *et al.* at 95-250 °C,[7] but utilizes substantially more volatile and reactive $Sb(SiMe_3)_3$ in place of $Sb(SiEt_3)_3$ (the former precursor is substantially less sterically hindered, given that it features 9 methyl groups in place of ethyl groups). The required precursor, $Sb(SiMe_3)_3$, was prepared as a colourless, pyrophoric and light-sensitive oil in 90% yield (Scheme 1) via the reaction of 3 equiv. of Na with Sb in 1,2-dimethoxyethane (in the presence of naphthalene as a catalyst) to form $Na_3Sb$, followed by the addition of 3 equiv. of $Me_3SiCl$. As an initial test of the feasibility of the proposed ALD method, the solution reactivity of $Sb(SiMe_3)_3$ with $SbCl_3$ was investigated. This reaction proceeded at room temperature in $C_6D_6$, affording a black precipitate of elemental antimony (confirmed by PXRD), accompanied by $Me_3SiCl$ as the only soluble byproduct (confirmed by $^1H$, $^{13}C$ and $^{29}Si$ NMR spectroscopy). The formation of $R_3SiCl$ as the solution reaction byproduct mirrors the observations of Pore *et al.* during ALD, who used *in situ* quadropole mass spectrometry (QMS) to identify the byproduct from the $Sb(SiEt_3)_3$/$SbCl_3$ ALD process as $Et_3SiCl$.[7]

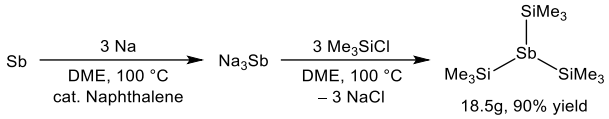


**Scheme 1.** Synthesis of $Sb(SiMe_3)_3$. DME= 1,2-dimethoxyethane.

To enable accurate temperature control, initial ALD experiments were carried out utilizing $Sb(SiMe_3)_3$ and $SbCl_3$ bubbler temperatures of 30 °C, and a substrate temperature of 35 °C. Substrates were hydrogen-terminated silicon (H-Si) and Si(100) with 100 nm of thermal oxide ($SiO_2$/Si). After 2000 ALD cycles using 0.1 s pulses, mirror-like films were obtained on both substrates, which were confirmed to be composed of elemental antimony by XPS and XRD. After sputtering to remove surface contaminants and antimony oxides, XPS revealed elemental antimony with low impurity levels (Figure 1). All peaks in the X-ray diffractograms (Figure 2) can be indexed to rhombohedral Sb (R-3m) with strong preferential orientation (i.e. crystallographic texture) apparent through the loss of some expected peaks and deviation of observed peaks from their ideal relative intensities. The resistivity of an Sb film grown on undoped $SiO_2$/Si using 3000 ALD cycles was 93 μΩ·cm (determined by 4-point probe), which is approximately double the literature value for bulk antimony (41.5 μΩ·cm),[45] and is comparable with the values (60-100 μΩ·cm) reported by Pore *et al.* for Sb films deposited using $Sb(SiEt_3)_3$/$SbCl_3$ at 95-200 °C.[7]

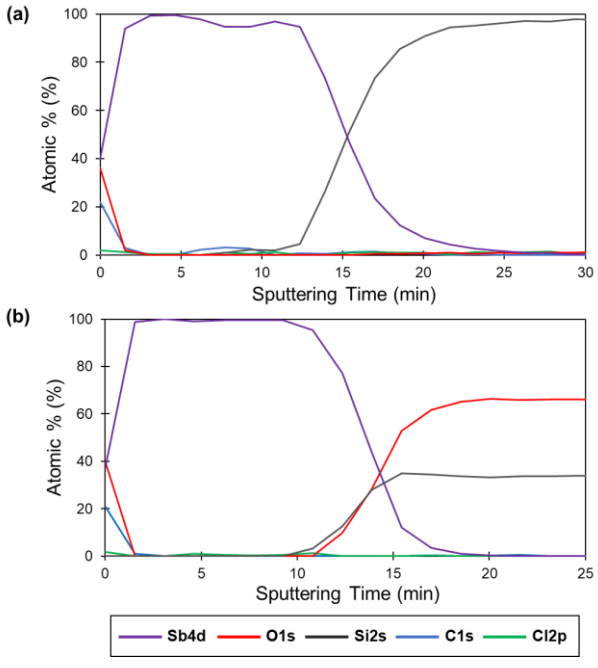


**Figure 1.** XPS depth analysis of Sb films grown on (a) H-Si and (b) $SiO_2$/Si at 35 °C using 2000 cycles and 0.1 second pulse times.

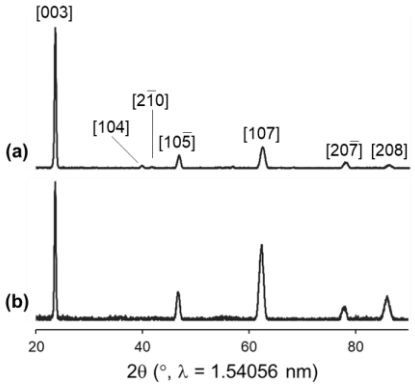


**Figure 2.** X-ray diffractograms of Sb films grown on (a) H-Si and (b) $SiO_2$/Si at 35 °C using 2000 cycles and 0.1 second pulse times.

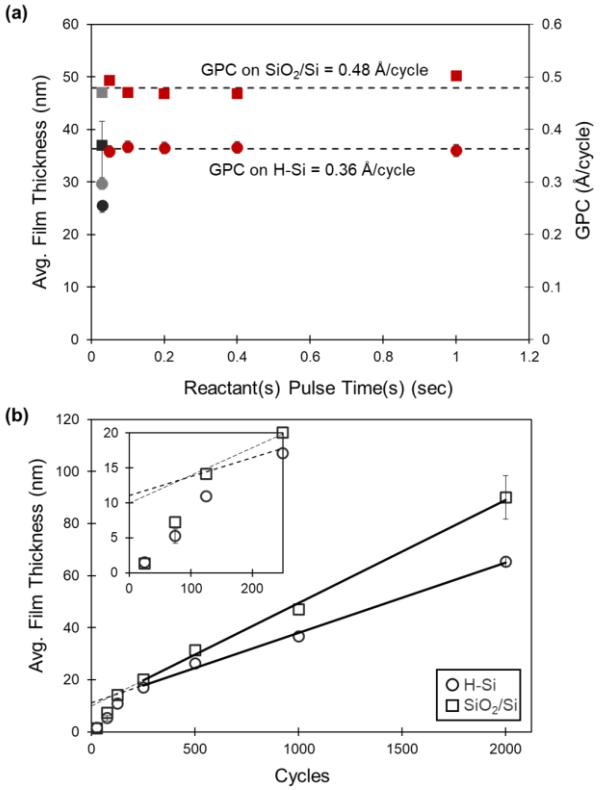


**Figure 3.** (a) Dependence of film thickness and GPC on $Sb(SiMe_3)_3$ and/or $SbCl_3$ pulse times for Sb deposition on H-Si (circles) and $SiO_2$/Si (squares). All experiments employed 1000 cycles and a deposition temperature of 35 °C. Red data points indicate experiments in which the pulse time (on the x-axis) applies to both $Sb(SiMe_3)_3$ and $SbCl_3$. Gray or black coloured data points indicate experiments in which the pulse time (on the x-axis) applies only to $Sb(SiMe_3)_3$ or $SbCl_3$, respectively (the pulse time of the other reactant was fixed at 0.1 s). (b) Dependence of film thickness on the number of cycles for Sb ALD on H-Si (circles) and $SiO_2$/Si (squares) substrates at 35 °C. Reactant pulse times were kept constant at 0.1 s. The inset shows an expanded view of the of the region from 0 to 250 cycles. In both (a) and (b), film thickness values are an average of 3 VASE measurements at different points on the surface of the wafer, and vertical bars depict the range of measured values (vertical bars are only shown if they extend more than 1 nm from the average value).

The conditions for self-limiting growth at 35 °C on $SiO_2$/Si and H-Si were assessed by varying the pulse lengths of both $Sb(SiMe_3)_3$ and $SbCl_3$ from 0.03 to 1.0 s (Figure 3a; 1000 cycles; variable angle spectroscopic ellipsometry (VASE) was used to determine film thickness). On $SiO_2$/Si, the growth rate remained constant at 0.48 Å/cycle using pulse times of at least 0.03 s and 0.05 s for $Sb(SiMe_3)_3$ and $SbCl_3$, respectively. On H-Si a growth rate of 0.36 Å/cycle was obtained utilizing $Sb(SiMe_3)_3$ and $SbCl_3$ pulses of at least 0.05 s. Sb deposition was also carried out with the bubblers and substrate at room temperature (23 °C), and self-limiting growth was verified through the observation of the same film thickness using precursor pulses of 0.1, 0.4 and 1.0 s, affording after 1000 cycles a GPC of 0.45 Å/cycle on $SiO_2$ and 0.37 Å/cycle on H-Si.

Film thickness varied linearly when the number of deposition cycles was varied from 125 to 2000 at 35 °C; Figure 3b. The y-axis intercept in this graph is greater than zero, indicative of a substrate-enhanced growth mechanism[46-52] in which a higher GPC is achieved during the initial growth phase (when substantial deposition is occurring on the $SiO_2$/Si or H-Si substrate surface, rather than the growing Sb film); experiments with 50-125 cycles afforded a GPC of 1.3 Å/cycle on $SiO_2$/Si, and 1.0 Å/cycle on H-Si (cf. 0.40 Å/cycle on $SiO_2$/Si, and 0.27 Å/cycle on H-Si for the region from 250-2000 cycles after the original substrate surface has been covered[53-56]). For films deposited using 500-2000 ALD cycles, continuous films were observed by SEM (films deposited on H-Si are shown in Figures 4 and S7; SEMs of films deposited on $SiO_2$/Si are provided in Figure S8). However, films deposited using 1000 or 2000 cycles on H-Si had increased surface roughness due to the formation of grains (100-300 nm in diameter) on the surface of the underlying antimony film; analogous behaviour was reported for Sb ALD at 95 °C using $Sb(SiEt_3)_3/SbCl_3$.[4] With 125 or 250 cycles, films composed of individual grains or grains in the process of coalescence, respectively, were observed.

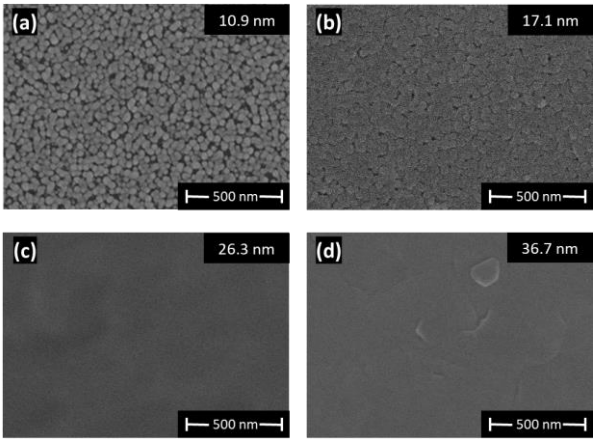


**Figure 4.** FESEM images of films grown on H-Si at 35 °C using (a) 125, (b) 250, (c) 500 and (d) 1000 ALD cycles. Film thicknesses are average values determined by VASE.

Deposition experiments were performed at temperatures ranging from 23 to 150 °C to determine the ALD window of the $Sb(SiMe_3)_3/SbCl_3$ process on $SiO_2$/Si and H-Si (Figure 5; 1000 cycles, 0.4 s precursor pulses). Film growth was observed at all temperatures with the highest GPC occurring at 65 °C (0.39

Å/cycle) on H-Si and 95 °C (0.53 Å/cycle) on $SiO_2$/Si. All films were shown to be composed of elemental Sb by XRD (Figures S11 and S14), as well as XPS for the film deposited on $SiO_2$/Si at 95 °C (Figure S16). However, films deposited above 95 °C on either substrate exhibited a decrease in the extent of crystallographic orientation relative to the substrate surface. On both substrates, ALD growth was found to occur up to 65 °C, as determined by an independence of growth rate on precursor pulse times (Figures S12 and S15) and the formation of reflective silver-coloured films (Figure S10) with uniform thickness by VASE. By contrast, films deposited at 95, 125 and 150 °C (using 0.4 s pulse times) appeared visibly non-uniform (Figure S10), and VASE indicated substantial variations in film thickness at different points on the wafer. These observations are inconsistent with ALD growth at 95-150 °C, and SEM also revealed a change in morphology, from smooth continuous films, to discontinuous grains (Figure S13).[57]

Consequently, the $Sb(SiMe_3)_3$/$SbCl_3$ ALD process is complementary to the previously reported $Sb(SiEt_3)_3$/$SbCl_3$ ALD process, in that the former enables low temperature (room temperature to 65 °C) deposition, whereas the latter operates at temperatures of 95°C and above. It is also notable that the low-temperature $Sb(SiMe_3)_3$/$SbCl_3$ ALD process (0.1s pulses) resulted in more effective nucleation on H-Si than ALD at 95 °C using $Sb(SiEt_3)_3$/$SbCl_3$ (2.0 s pulses; Figures S24-25). This could perhaps be due to improved physisorption at low temperature, or the greater reactivity and reduced steric bulk of $Sb(SiMe_3)_3$ versus $Sb(SiEt_3)_3$.

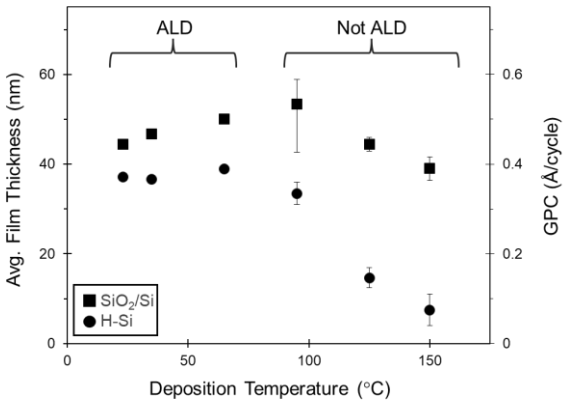


**Figure 5.** Dependence of film thickness and GPC on Sb deposition temperature on H-Si (circles) and $SiO_2$/Si (squares). All films were deposited using 1000 cycles and 0.4 second reactant pulse times. Film thickness values are an average of 3 VASE measurements at different points on the surface of the wafer, and vertical bars depict the range of measured values (vertical bars are only shown if they extend more than 1 nm from the average value).

As illustrated in Figures 6a and S7-8, films deposited at 35 °C using ≤250 ALD cycles were composed of isolated grains. However, we wondered whether in-situ pre-treatment of the H-Si or $SiO_2$/Si surface with $Sb(SiMe_3)_3$ or $SbCl_3$ might generate additional nucleation sites leading to more continuous film growth at low cycle numbers. Consequently, the surface was treated with 50 × 0.1-0.8 s pulses of $Sb(SiMe_3)_3$ or $SbCl_3$ prior to carrying out 50 ALD cycles (Figures S17-20; the reactor was placed under vacuum for 2-5 minutes between pre-treatment and ALD; use of an additional 20 minute argon purge between pre-treatment and the start of ALD afforded nearly identical film thicknesses;[58] no film deposition was observed by VASE after surface pre-treatment alone). In these experiments, significantly more continuous films were obtained using 50 x 0.4 s pulses of $Sb(SiMe_3)_3$ or $SbCl_3$ as the pre-treatment, and 0.4 s pulses during ALD (b and d in Figure 6). Additionally, films of the same thickness, but with further improved surface coverage, were obtained using 50 x 0.8 s pulses of $Sb(SiMe_3)_3$ or $SbCl_3$ as the pre-treatment, and 0.8 s pulses during ALD (c and e in Figure 6). For example, on H-Si, a continuous 6.7 nm thick film was produced after initial pre-treatment with 50 x 0.8 s pulses of $SbCl_3$, followed by 50 ALD cycles using 0.8 s pulses.

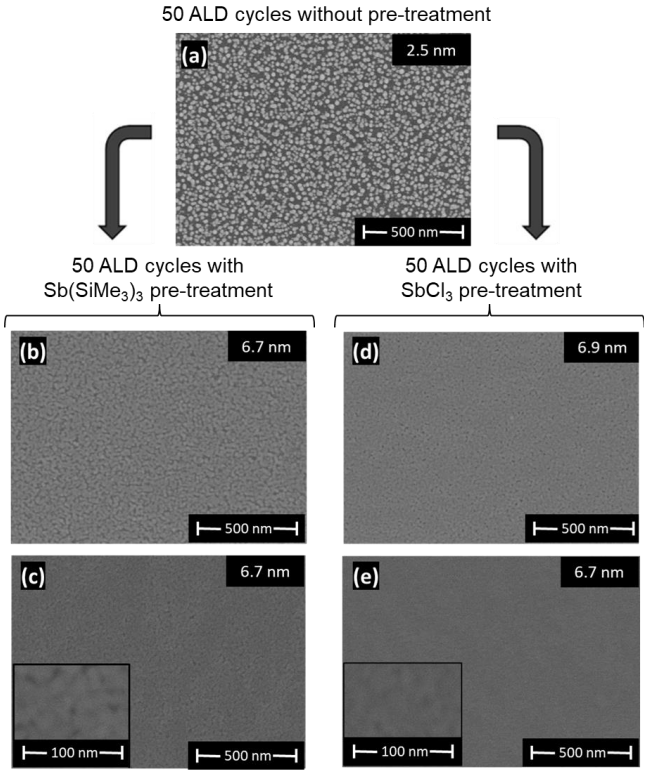


**Figure 6.** FESEM images of films grown on H-Si at 35 °C with or without 50 pulses of $Sb(SiMe_3)_3$ or $SbCl_3$ prior to carrying out 50 ALD cycles: (a) 50 ALD cycles (0.1 s pulses) without any pre-treatment, (b) pre-treatment with $Sb(SiMe_3)_3$ (50 × 0.4 s pulses), followed by 50 ALD cycles (using 0.4 s pulses), (c) pre-treatment with $Sb(SiMe_3)_3$ (50 × 0.8 s pulses), followed by 50 ALD cycles (using 0.8 s pulses), (d) pre-treatment with $SbCl_3$ (50 × 0.4 s pulses), followed by 50 ALD cycles (using 0.4 s pulses), and (e) pre-treatment with $SbCl_3$ (50 × 0.8 s pulses), followed by 50 ALD cycles (using 0.8 s pulses). Film thicknesses are average values determined by VASE.

The use of longer ALD pulses in the first 50 ALD cycles after surface pre-treatment is likely required in order to achieve complete reactivity with an increased density of reactive surface sites. The effect of surface pre-treatment and longer ALD pulses during the first 50 cycles was probed by carrying out depositions (at 35 °C) utilizing 50 x 0.4 s pulses of $Sb(SiMe_3)_3$ or $SbCl_3$ for pre-treatment, followed by between 50 and 2000 ALD cycles, where the first 50 cycles utilized 0.4 s precursor pulses, and any remaining cycles utilized 0.1 s precursor pulses. Plots of film thickness versus cycle number are provided in Figure 7 for deposition on H-Si, and Figure S22 for deposition on $SiO_2$/Si. These plots indicate that during the initial ALD growth phase (the first ~125 cycles) surface pre-

treatment results in a further increased GPC, but after this point, the GPC matches that for depositions carried out without the use of surface pre-treatment. However, it is interesting to note that films deposited using surface pre-treatment prior to ALD (35 °C; 2000 cycles) exhibited a change in crystallographic texture (for X-ray diffractograms, see Figures 8 and S21). The resistivities of films obtained using initial $SbCl_3$ or $Sb(SiMe_3)_3$ pre-treatment (35 °C; undoped $SiO_2$/Si substrates; 2000 ALD cycles) were 91 μΩ·cm and 98 μΩ·cm, respectively (cf. 93 μΩ·cm for the film deposited without pre-treatment).

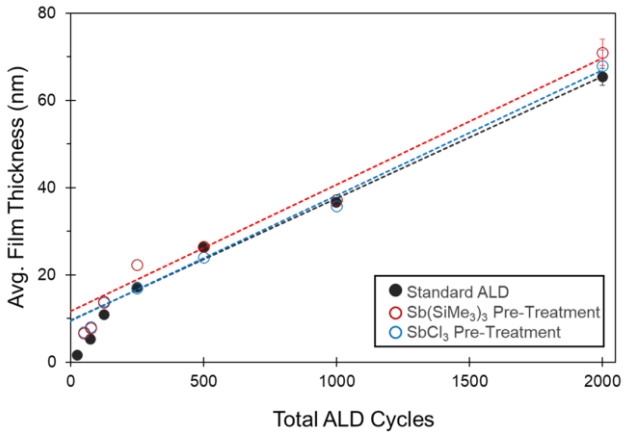


**Figure 7.** Film thickness versus the number of ALD cycles for 35 °C deposition on H-Si using: (i; black) standard ALD parameters (no pre-treatment, all cycles using 0.1 s pulses), (ii; red) ALD with $Sb(SiMe_3)_3$ pre-treatment (surface pre-treatment with 50 x 0.4 s pulses of $Sb(SiMe_3)_3$, followed by 50 ALD cycles using 0.4 s pulses, and all remaining ALD cycles using 0.1 s pulses), or (iii; blue) ALD with $SbCl_3$ pre-treatment (surface pre-treatment with 50 x 0.4 s pulses of $SbCl_3$, followed by 50 ALD cycles using 0.4 s pulses, and all remaining ALD cycles using 0.1 s pulses).

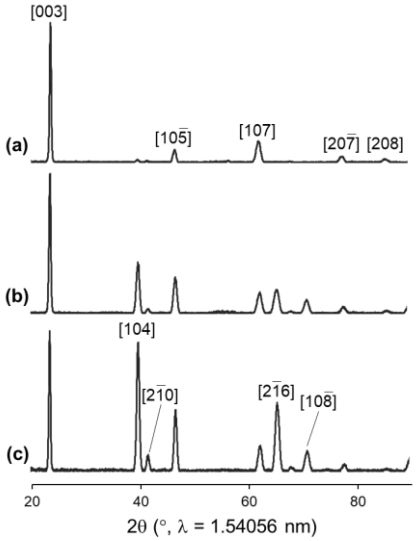


**Figure 8.** X-ray diffractograms of Sb films grown on H-Si (35 °C; 2000 cycles) using (a) the standard ALD method (no pre-treatment, all 0.1 s precursor pulses), (b) ALD with $Sb(SiMe_3)_3$ pre-treatment (surface pre-treatment with 50 x 0.4 s pulses of $Sb(SiMe_3)_3$, followed by 50 ALD cycles using 0.4 s pulses, and then 1950 cycles using 0.1 s pulses), or (c) ALD with $SbCl_3$ pre-treatment (surface pre-treatment with 50 x 0.4 s pulses of $SbCl_3$, followed by 50 ALD cycles using 0.4 s pulses, and then 1950 cycles using 0.1 s pulses).

## SUMMARY AND CONCLUSIONS

Room temperature thermal ALD of elemental antimony was achieved using $Sb(SiMe_3)_3$ and $SbCl_3$. This was made possible by (a) the high volatility of both precursors, which enables room temperature delivery (using a reactor pressure of ~1.0 Torr), (b) the high reactivity of this precursor combination, which facilitates rapid surface-based reactivity within each ALD cycle, and (c) the volatility of the $Me_3SiCl$ reaction byproduct, which enables efficient byproduct removal from the surface of the growing film, even at room temperature.

Antimony ALD had previously been reported in the 95-250 °C range (with self-limiting growth demonstrated at 95 °C) using $SbCl_3$ in combination with $Sb(SiEt_3)_3$,[7] which is less volatile and less reactive than $Sb(SiMe_3)_3$. The $Sb(SiMe_3)_3$/$SbCl_3$ ALD process provided uniform films of crystalline antimony on H-Si or $SiO_2$/Si in the temperature range of 23-65 °C. On $SiO_2$/Si substrates, ALD using $Sb(SiMe_3)_3$/$SbCl_3$ at 35 °C afforded films with a similar morphology and thickness to those deposited using $Sb(SiEt_3)_3$/$SbCl_3$ at 95 °C. By contrast, on hydrogen terminated silicon (H-Si), improved nucleation was achieved using the former low-temperature process.

Film growth using $Sb(SiMe_3)_3$/$SbCl_3$ at 35 °C proceeded via a substrate-enhanced growth mechanism[46-48] in which a higher GPC is achieved during the initial growth phase (when substantial deposition is occurring on the $SiO_2$/Si or H-Si substrate surface, rather than the growing Sb film). The use of 250 ALD cycles, or less, afforded films composed of isolated grains. However, in this initial growth stage, in-situ surface pre-treatment by $Sb(SiMe_3)_3$ or $SbCl_3$ (50 x 0.4 or 0.8 s pulses) combined with the use of longer precursor pulses (0.4 or 0.8 s) during the first 50 ALD cycles resulted in improved nucleation. For example, on H-Si, a continuous 6.7 nm thick film was produced after initial pre-treatment with 50 x 0.8 s pulses of $SbCl_3$, followed by 50 ALD cycles using 0.8 s pulses. The use of longer ALD pulses in the first 50 ALD cycles after surface pre-treatment is likely required in order to achieve complete reactivity with an increased density of reactive surface sites.

ALD processes capable of operating at room temperature are scarce, and to the best of our knowledge, a pure element has not previously been deposited by thermal ALD (with demonstrated self-limiting growth) at room temperature. Room temperature ALD processes are of particular interest as a means to enable deposition on thermally-sensitive substrates,[27] to minimize problems with agglomeration of low-melting films (e.g. Cu),[36] and to enable ALD using less complex (and less expensive) ALD reactors. Room temperature thermal ALD methods can also be beneficial for high-throughput roll-to-roll ALD techniques,[27] and for area-selective ALD using small molecule inhibitors,[37] where inhibitor desorption and undesired reactivity can be minimized at low temperature.

Thin (<10 nm) ALD-grown antimony films may find applications in monoatomic phase change memory, nanophotonics, optoelectronics, or for the preparation of antimony-doped silicon or germanium.

## EXPERIMENTAL SECTION

**General Details:** An argon-filled Innovative Technology Pure-Lab HE glovebox equipped with a −30 °C freezer was employed for the manipulation and storage of all oxygen- and moisture-sensitive compounds. Air-sensitive syntheses were performed

on a double-manifold high-vacuum line (with mercury bubblers) equipped with an Edwards R12 vacuum pump using standard techniques. The vacuum was measured periodically using a Kurt J. Lesker 275i convection enhanced Pirani gauge. Commonly utilized specialty glassware included thick-walled flasks equipped with Teflon taps leading to a 24/40 glass joint (bombs), or J. Young or Wilmad LPV NMR tubes. Centrifugation was performed using a Fisher Scientific model 228 centrifuge [using Kimble 15 mL glass centrifuge tubes (21020-684) and Wheaton PTFE-lined phenolic caps (240463)] located within the glovebox. Argon cylinders (Linde) of 99.998% and 99.999% purity were used for the ALD reactor and vacuum lines, respectively. Argon supplied to the vacuum lines was purified to below 0.1 ppm of $O_2$ and 0.5 ppm $H_2O$ using an Oxisorb-W scrubber from Matheson Gas Products. Argon supplied to the ALD reactor was purified to below 100 ppt of $O_2$ and $H_2O$ using an SAES MC450-902F purifier.

1,2-Dimethoxyethane (DME) was purchased from Sigma-Aldrich, hexanes was purchased from Caledon, and deuterated benzene was purchased from Cambridge Isotope Laboratories. All solvents were initially dried over an appropriate drying agent (DME = 4 Å mol. sieves followed by $Na/Ph_2CO$; hexanes = $Na/Ph_2CO$/tetraglyme; $C_6D_6$ = $Na/Ph_2CO$), and then distilled. Antimony powder, sodium, naphthalene, $Me_3SiCl$, and $SbCl_3$ were purchased from Sigma-Aldrich and stored under argon. All reagents were used without further purification. 48% HF (used to prepare 2% HF solutions), 30% $H_2O_2$, and conc. $H_2SO_4$ were purchased from Sigma-Aldrich. Ultrapure water (UPW) was produced using a Milli-Q Direct Water Purification System. Plasma cleaning was carried out using a Basic Plasma Cleaner (PDC-32G) from Harrick Plasma connected to a 3.6 cfm Edwards nXDS6i scroll pump. A leak valve (to air) was used to set the pressure in the plasma cleaner to 600-650 mTorr during plasma cleaning (RF coil set to 18 W).

Solution NMR spectroscopy was performed on a Bruker AV-600 spectrometer at 298 K. All $^1H$ and $^{13}C$ NMR spectra were referenced relative to $SiMe_4$ through the resonance of the protio impurity in $C_6D_6$ (for $^1H$ NMR; 7.16 ppm) or the resonance of $C_6D_6$ (for $^{13}C$ NMR; 128.06 ppm). $^{29}Si$ NMR spectra were indirectly referenced by conversion of the spectral frequency of the $^1H$ NMR spectrum using the frequency ratio of $^1H$ and $^{29}Si$, as described by Harris et al.[59]

**Tris(trimethylsilyl)antimony:** $Sb(SiMe_3)_3$ was prepared using a modification of the previously reported syntheses,[60,61] based on the syntheses of $Sb(SiEt_3)_3$[7] and $Sb(Si^iPr_3)_3$[62] (note: all work conducted outside of a glove box was carried out in a fume hood): In a thick-walled 500 mL bomb, a mixture of Sb powder (7.35 g; 0.060 mol), thin ribbons of Na (4.18 g; 0.182 mol) and naphthalene (300 mg; 2.34 mmol) in DME (200 mL) was stirred at 100 °C for 2 days to afford a black-coloured slurry of $Na_3Sb$. After cooling to room temperature, trimethylchlorosilane (27 mL; 0.213 mol) was added dropwise with vigorous stirring over 30 minutes. The mixture then heated at 100 °C for 3 days. The volume of the black slurry was halved in vacuo, before the mixture was brought into a glovebox and centrifuged. The solid residue was washed with 30 mL of hexanes, followed by centrifugation. The combined mother liquors were transferred to a 250 mL bomb, attached to a vacuum line, and cooled to 0 °C. Remaining solvent was slowly distilled from the solution (through the vacuum line) into a receiving bomb cooled to −78 °C under static vacuum. This afforded $Sb(SiMe_3)_3$ as a pale yellow oil (18.5 g, 0.054 mol, 90%), which was brought into a glovebox and stored at −30 °C as a solid. $Sb(SiMe_3)_3$ is light sensitive and seemingly reactive towards polypropylene centrifuge tubes (presumably due to reaction with additives). Therefore, glass centrifuge tubes should be used, and $Sb(SiMe_3)_3$ should be stored in the dark. $^1H$ NMR ($C_6D_6$): δ = 0.43 ppm (s); $^{13}C\{^1H\}$ NMR: δ = 5.03 ppm; $^{29}Si$ NMR: δ = −8.68 ppm. *Caution: $Sb(SiMe_3)_3$ is pyrophoric and the toxicity of this compound (and intermediates involved in the synthesis) is unknown. This synthesis should only be attempted in a well-ventilated fume hood by trained chemists with appropriate infrastructure and experience in the preparation and handling of highly air-sensitive chemicals.*

**ALD Experiments:** All ALD experiments were conducted in a home-built ALD reactor. The reactor consists of a reaction chamber (a 4.5" conflat cube) housed within an oven. This reaction chamber contains a flange-mounted 1-inch heated substrate stage (Heatwave labs) which can be heated independently to a temperature equal to or above the temperature of the surrounding oven. The reaction chamber is connected to an Edwards R12 vacuum pump (located within a fume hood) via a heated foreline (a section is heated to ~300 °C, but most of the foreline is at 100-150 °C) with several manual bellows valves, and a 4 Å molecular sieve trap (MDC vacuum products) to prevent oil backstreaming from the pump. The foreline also connects to a Convection Enhanced Pirani Vacuum Gauge (not connected during ALD). Four separate precursor lines attach to the top of the reaction chamber. One line can be used for room temperature precursor delivery. One can be used for gaseous precursor delivery. Two lines lead to heated bubblers of a flow-through design (but with a dip tube short enough to avoid contact with the precursor upon initial loading of the bubbler; see Figure S29); one heated bubbler is housed within the same oven that contains the reaction chamber, while the second is housed in an adjacent oven (connected to the oven that contains the reaction chamber via a short section of tubing which can be independently heated). Purified argon is supplied to each of the four precursor lines via a mass flow controller and pneumatically actuated diaphragm valve. For all ALD experiments, argon flows of 50 sccm were used on the two unused lines, and flows of 200 sscm were used on the two in-use lines, resulting in a reactor pressure of ~1.0 Torr during ALD.

The $SbCl_3$ and $Sb(SiMe_3)_3$ bubblers[63] were maintained at 30 °C in all experiments except for room temperature deposition experiments in which all heaters were turned off. Substrate temperatures ranged from room temperature (~23 °C) to 150 °C. For all depositions in this work, the purge time following each precursor pulse was 30 s (the ALD reactor used in this work requires longer pulses than most commercial ALD reactors due to the significantly larger reaction chamber volume). Note: the GPC for the $Sb(SiMe_3)_3/SbCl_3$ ALD process (at 35 °C) shows significant dependence on purge duration, as shown in Figure S23. This is presumably due to some desorption of weakly adsorbed precursor during the purge step, and analogous behaviour was previously observed, by in-situ QCM, for Sb ALD using $Sb(SiEt_3)_3/SbCl_3$ at 98 °C.[7] Analogous behaviour was also observed during $Sb_2Te_3$ ALD using $Te(SiEt_3)_2/SbCl_3$.[64,65]

**ALD Substrates:** All ALD experiments used double side polished Si(100) wafers with a layer (100 or 2 nm) of oxide, or freshly prepared hydrogen-terminated Si(100) substrates. Si(100) substrates with a layer of oxide ($SiO_2$/Si) were plasma cleaned (air plasma) for 10 minutes immediately prior to being loaded into the ALD reactor and placed under vacuum. Hydrogen-terminated Si(100) (H-Si) substrates were prepared using the following procedure: 1 cm x 1 cm sections of a Si(100) wafer with a ≤5 nm of native oxide were placed in beaker containing 85 °C piranha (3:1 $H_2O_2/H_2SO_4$) for 10 minutes, followed by

a quick rinse under a stream of UPW. The wafer was then placed in a PTFE beaker containing 2% $HF_{(aq)}$ for 1-2 minutes,[66-68] rinsed in a stream of UPW, and dried under a rapid flow of nitrogen or argon. The wafer was then quickly (within 2 or 3 minutes) loaded into the ALD reactor and placed under vacuum.

**Solid-State Characterization:** Powder and thin film X-ray diffraction (XRD) was carried out using a Bruker D8 Discover diffractometer equipped with a Vantec 500 area detector and a focused Cu source with $K_\alpha$ radiation ($\lambda$ = 1.5418 Å) operated at 40 kV and 40 mA. Thin films were measured using a 2θ scan with Φ rotation and a fixed θ angle of 5° (6 frames with exposure times of 300 seconds per frame) to produce a continuous 2θ range of 10-130°. Powders were measured using a coupled θ-2θ scan with Φ rotation (6 frames with exposure times of 300 seconds per frame) to produce a continuous 2θ range of 10-130°. A reference Sb diffractogram was produced using Mercury software with data retrieved from the Inorganic Crystal Structure Database (ICSD collection code 64695). Experimental diffractograms were generated and analyzed using GADDS, Diffrac.EVA, and Topas.

Average film thicknesses were determined by variable angle spectroscopic ellipsometry (VASE) using a J. A. Woolam M-2000 spectroscopic ellipsometer. Measurements were taken from 55° to 75° at 5° increments with an acquisition time of 10 seconds. Experimental data were modeled using the CompleteEase software provided with the spectrometer. For films deposited on $SiO_2$/Si, the model used to fit the experimental data consisted of a Si substrate with a $SiO_2$ layer of fixed thickness (thickness determined by VASE analysis of the bare substrates) followed by a B-Spline model with starting material parameters set to Sb. Films deposited on H-Si were treated analogously, but without the $SiO_2$ layer in the model. Models utilized data obtained in the angle and wavelength ranges 65-70° and 300-900 nm. In all cases, VASE measurements were carried out at 3 points on the wafer, and quoted thickness values are an average of all three measurements (where film thickness data is represented graphically, vertical lines indicate the range of the 3 obtained values; only shown if the range extends > 1 nm from the average value). Average thickness values from VASE were periodically confirmed by AFM step analysis (immediately before placing inside the reaction chamber, a strip of 1/8" wide Kapton tape was neatly stuck to one side of the substrate; after deposition, the tape was peeled off to reveal the bare substrate, which was cleaned with isopropanol and hexanes to remove any tape residue) and/or cross-sectional SEM.

In addition to XRD, film composition was analyzed by X-ray photoelectron spectroscopy (XPS) using a Thermofisher Scientific Escalab 250Xi (monochromatic Al-Kα source) with a nominal spot size of 900 μm. Sputtering depth profiles were obtained using 2000 eV monoatomic $Ar^+$ ion bombardment at a high current density with a 90 sec cycle time rastered over an area of 4.5 mm by 4.5 mm. Electron micrographs were obtained using a FEI Magellan 400 and analyzed using ImageJ. All thickness values depicted on the top right corner of FESEM images were obtained from VASE. Atomic force micrographs were obtained using a Bruker Dimension Icon AFM and analyzed using Nanoscope Analysis software. Surface resistivity of selected films (those deposited on undoped Si(100) wafers with 2 nm of oxide) were measured using a Jandel cylindrical four-point-probe (CYL-1.0-45-TC-250-8; 1 mm tip spacing; tungsten carbide tips with 0.25mm tip radius) and Jandel HM20 4PP test meter.

## ASSOCIATED CONTENT

### Supporting Information

The Supporting Information for this paper (NMR spectra, X-ray diffractograms, XPS data, FESEM images, photographs of films, plots of film thickness versus pulse length, number of cycles, or purge time, AFM step analysis, VASE data, and a photograph of the type of bubbler used in this work) is available free of charge on the ACS Publications website.

## AUTHOR INFORMATION

### Corresponding Author

*D.J.H.E.: tel, 905-525-9140 x23307; fax, 905-522-2509; e-mail, emslied@mcmaster.ca.

### Notes

The authors declare no competing financial interest.

## ACKNOWLEDGMENT

D.J.H.E. thanks NSERC of Canada for a Discovery Grant, Intel Corporation for funding support via the Semiconductor Research Corporation, and the Ontario government for an Ontario Research Fund Research Excellence (ORF-RE) grant. M.A.H. thanks NSERC of Canada for PGS-D award. We are grateful to Dr. Rana N. S. Sodhi at Surface Interface Ontario (Toronto) for performing XPS, Chris Butcher at the Canadian Centre for Electron Microscopy for obtaining FESEM images, and to Victoria M. Jarvis and Dr. James F. Britten in the McMaster X-ray diffraction facility for helpful crystallographic discussions. Additionally, we thank Nicholas Hoffman in the Emslie group for obtaining AFM images.

## REFERENCES

(1) Miikkulainen, V.; Leskelä, M.; Ritala, M.; Puurunen, R. L. Crystallinity of inorganic films grown by atomic layer deposition: Overview and general trends, *J. Appl. Phys.* **2013**, *113*, 021301.

(2) Hagen, D. J.; Pemble, M. E.; Karppinen, M. Atomic layer deposition of metals: Precursors and film growth, *Appl. Phys. Rev.* **2019**, *6*, 041309.

(3) Emslie, D. J. H.; Chadha, P.; Price, J. S. Metal ALD and pulsed CVD: Fundamental reactions and links with solution chemistry, *Coord. Chem. Rev.* **2013**, *257*, 3282-3296.

(4) Knisley, T. J.; Kalutarage, L. C.; Winter, C. H. Precursors and chemistry for the atomic layer deposition of metallic first row transition metal films, *Coord. Chem. Rev.* **2013**, *257*, 3222-3231.

(5) Blakeney, K. J.; Winter, C. H. Atomic Layer Deposition of Aluminum Metal Films Using a Thermally Stable Aluminum Hydride Reducing Agent, *Chem. Mater.* **2018**, *30*, 1844-1848.

(6) Stevens, E. C.; Mousa, M. B. M.; Parsons, G. N. Thermal atomic layer deposition of Sn metal using $SnCl_4$ and a vapor phase silyl dihydropyrazine reducing agent, *J. Vac. Sci. Technol., A* **2018**, *36*, 06A106.

(7) Pore, V.; Knapas, K.; Hatanpää, T.; Sarnet, T.; Kemell, M.; Ritala, M.; Leskelä, M.; Mizohata, K. Atomic Layer Deposition of Antimony and its Compounds Using Dechlorosilylation Reactions of Tris(triethylsilyl)antimony, *Chem. Mater.* **2011**, *23*, 247-254.

(8) Cheng, L. X.; Adinolfi, V.; Weeks, S. L.; Barabash, S. V.; Littau, K. A. Conformal deposition of GeTe films with tunable Te composition by atomic layer deposition, *J. Vac. Sci. Technol., A* **2019**, *37*, 020907.

(9) Salinga, M.; Kersting, B.; Ronneberger, I.; Jonnalagadda, V. P.; Vu, X. T.; Le Gallo, M.; Giannopoulos, I.; Cojocaru-Mirédin, O.; Mazzarello, R.; Sebastian, A. Monatomic phase change memory, *Nat, Mater.* **2018**, *17*, 681-685.

(10) Zhang, W.; Ma, E. Single-element glass to record data, *Nat, Mater.* **2018**, *17*, 654-655.

(11) Hu, Y. F.; Qiu, Q. Q.; Zhu, X. Q.; Lai, T. S. Ultrafast crystallization in nanoscale phase change film of monobasic antimony, *Appl. Surf. Sci.* **2020**, *505*, 144337.

(12) Jiao, F. Y.; Chen, B.; Ding, K. Y.; Li, K. L.; Wang, L.; Zeng, X. R.; Rao, F. Monatomic 2D phase-change memory for precise neuromorphic computing, *Applied Materials Today* **2020**, *20*, 100641.

(13) Xu, J. B.; Hu, Y. F.; Lai, T. S.; Xu, Y. K.; Sun, S. Improved thermal stability and contact of antimony film by the interlayer $HfO_2$, *Journal of Materials Science-Materials in Electronics* **2020**, *31*, 8052-8058.

(14) Noé, P.; Vallée, C.; Hippert, F.; Fillot, F.; Raty, J.-Y. Phase-change materials for non-volatile memory devices: from technological challenges to materials science issues, *Semicond. Sci. Technol.* **2018**, *33*, 013002.

(15) Wuttig, M.; Bhaskaran, H.; Taubner, T. Phase-change materials for non-volatile photonic applications, *Nature Photonics* **2017**, *11*, 465-476.

(16) For a review on the use of ALD to deposit phase change memory materials, see: Lee, Y. K.; Yoo, C.; Kim, W.; Jeon, J. W.; Hwang, C. S. Atomic layer deposition of chalcogenides for next-generation phase change memory, *J. Mater. Chem. C* **2021**, *9*, 3708-3725.

(17) Cheng, Z. G.; Milne, T.; Salter, P.; Kim, J. S.; Humphrey, S.; Booth, M.; Bhaskaran, H. Antimony thin films demonstrate programmable optical nonlinearity, *Science Advances* **2021**, *7*, eabd7097.

(18) Ye, L.; de Jong, M. P.; Kudernac, T.; van der Wiel, W. G.; Huskens, J. Doping of semiconductors by molecular monolayers: monolayer formation, dopant diffusion and applications, *Mater. Sci. Semicond. Process* **2017**, *62*, 128-134.

(19) O'Connell, J.; Biswas, S.; Duffy, R.; Holmes, J. D. Chemical approaches for doping nanodevice architectures, *Nanotechnology* **2016**, *27*, 342002.

(20) Zhang, C. F.; Chang, S. N.; Dan, Y. P. Advances in ultrashallow doping of silicon, *Adv. Phys.: X* **2021**, *6*, 1871407.

(21) Most MLD studies have focused on phosphorus or boron as the dopant. However, monolayer doping (MLD) of germanium by antimony has been reported: see ref. 22. Additionally, related nanometer-scale doping of silicon with antimony has been described: see ref. 23.

(22) Alphazan, T.; Alvarez, A. D.; Martin, F.; Grampeix, H.; Enyedi, V.; Martinez, E.; Rochat, N.; Veillerot, M.; Dewitte, M.; Nys, J. P.; Berthe, M.; Stievenard, D.; Thieuleux, C.; Grandidier, B. Shallow Heavily Doped n++ Germanium by Organo-Antimony Monolayer Doping, *ACS Appl. Mater. Interfaces* **2017**, *9*, 20179-20187.

(23) Popere, B. C.; Russ, B.; Heitsch, A. T.; Trefonas, P.; Segalman, R. A. Large-Area, Nanometer-Scale Discrete Doping of Semiconductors via Block Copolymer Self-Assembly, *Advanced Materials Interfaces* **2015**, *2*, 1500421.

(24) Carbon-free monolayer doping (MLD) of an OH-terminated silicon surface was recently achieved using $PCl_3$ as the dopant-carrying molecule: Li, K.; Zhang, J. Y.; Chang, S. N.; Wei, H.; Zhang, J. J.; Dan, Y. P. Full Activation of Dopants by Carbon-free Self-Assembled Molecular Monolayer Doping, *ACS Appl. Electron. Mater.* **2021**, *3*, 3346-3351.

(25) For doping of silicon with boron via MLD, an elegant strategy to increase the level of doping involved the use of carborane clusters containing ten boron atoms: Ye, L.; Gonzalez-Campo, A.; Nunez, R.; de Jong, M. P.; Kudernac, T.; van der Wiel, W. G.; Huskens, J. Boosting the Boron Dopant Level in Monolayer Doping by Carboranes, *ACS Appl. Mater. Interfaces* **2015**, *7*, 27357-27361.

(26) Nam, T.; Kim, J. M.; Kim, M. K.; Kim, H.; Kim, W. H. Low-temperature Atomic Layer Deposition of $TiO_2$, $Al_2O_3$, and ZnO Thin Films, *J. Korean Phys. Soc.* **2011**, *59*, 452-457.

(27) Potts, S. E.; Profijt, H. B.; Roelofs, R.; Kessels, W. M. M. Room-Temperature ALD of Metal Oxide Thin Films by Energy-Enhanced ALD, *Chem. Vap. Deposition* **2013**, *19*, 125-133.

(28) Putkonen, M.; Niinisto, L. Atomic layer deposition of $B_2O_3$ thin films at room temperature, *Thin Solid Films* **2006**, *514*, 145-149.

(29) Pilli, A.; Jones, J.; Lee, V.; Chugh, N.; Kelber, J.; Pasquale, F.; LaVoie, A. In situ XPS study of low temperature atomic layer deposition of $B_2O_3$ films on Si using $BCl_3$ and $H_2O$ precursors, *J. Vac. Sci. Technol., A* **2018**, *36*, 061503.

(30) Ferguson, J. D.; Smith, E. R.; Weimer, A. W.; George, S. M. ALD of $SiO_2$ at room temperature using TEOS and $H_2O$ with $NH_3$ as the catalyst, *J. Electrochem. Soc.* **2004**, *151*, G528-G535.

(31) Arl, D.; Roge, V.; Adjeroud, N.; Pistillo, B. R.; Sarr, M.; Bahlawane, N.; Lenoble, D. $SiO_2$ thin film growth through a pure atomic layer deposition technique at room temperature, *RSC Adv.* **2020**, *10*, 18073-18081.

(32) Thermal ALD of tungsten has been reported at 152-327 °C (using $WF_6$/$Si_2H_6$). Room temperature tungsten deposition (using $WF_6$/$Si_2H_6$) was also investigated, but extremely long $WF_6$ pulses were required to achieve saturation, and the authors noted that the $WF_6$ reaction did not proceed to completion. See refs. 33 and 34.

(33) Klaus, J. W.; Ferro, S. J.; George, S. M. Atomic layer deposition of tungsten using sequential surface chemistry with a sacrificial stripping reaction, *Thin Solid Films* **2000**, *360*, 145-153.

(34) Elam, J. W.; Nelson, C. E.; Grubbs, R. K.; George, S. M. Kinetics of the $WF_6$ and $Si_2H_6$ surface reactions during tungsten atomic layer deposition, *Surf. Sci.* **2001**, *479*, 121-135.

(35) Room temperature copper deposition by an ALD-like process has been reported (using $Cu(hfac)_2$/pyridine/$H_2$), but self-limiting growth was not demonstrated: Kang, S.-W.; Yun, J.-Y.; Chang, Y. H. Growth of Cu Metal Films at Room Temperature Using Catalyzed Reactions, *Chem. Mater.* **2010**, *22*, 1607-1609.

(36) Guo, Z.; Li, H.; Chen, Q.; Sang, L. J.; Yang, L. Z.; Liu, Z. W.; Wang, X. W. Low-Temperature Atomic Layer Deposition of High Purity, Smooth, Low Resistivity Copper Films by Using Amidinate Precursor and Hydrogen Plasma, *Chem. Mater.* **2015**, *27*, 5988-5996.

(37) Parsons, G. N.; Clark, R. D. Area-Selective Deposition: Fundamentals, Applications, and Future Outlook, *Chem. Mater.* **2020**, *32*, 4920-4953.

(38) Yarbrough, J.; Shearer, A. B.; Bent, S. F. Next generation nanopatterning using small molecule inhibitors for area-selective atomic layer deposition, *J. Vac. Sci. Technol., A* **2021**, *39*, 021002.

(39) Hwang, Y.; Nguyen, B. M.; Dayeh, S. A. Atomic layer deposition of platinum with enhanced nucleation and coalescence by trimethylaluminum pre-pulsing, *Appl. Phys. Lett.* **2013**, *103*, 263115.

(40) de Paula, C.; Richey, N. E.; Zeng, L.; Bent, S. F. Mechanistic Study of Nucleation Enhancement in Atomic Layer Deposition by Pretreatment with Small Organometallic Molecules, *Chem. Mater.* **2020**, *32*, 315-325.

(41) de Paula, C.; Bobb-Semple, D.; Bent, S. F. Increased selectivity in area-selective ALD by combining nucleation enhancement and SAM-based inhibition, *J. Mater. Res.* **2021**, *36*, 582-591.

(42) Minjauw, M. M.; Rijckaert, H.; Van Driessche, I.; Detavemier, C.; Dendooven, J. Nucleation Enhancement and Area-Selective Atomic Layer Deposition of Ruthenium Using $RuO_4$ and $H_2$ Gas, *Chem. Mater.* **2019**, *31*, 1491-1499.

(43) Khan, R.; Shong, B.; Ko, B. G.; Lee, J. K.; Lee, H.; Park, J. Y.; Oh, I. K.; Raya, S. S.; Hong, H. M.; Chung, K. B.; Luber, E. J.; Kim, Y. S.; Lee, C. H.; Kim, W. H.; Lee, H. B. R. Area-Selective Atomic Layer Deposition Using Si Precursors as Inhibitors, *Chem. Mater.* **2018**, *30*, 7603-7610.

(44) Liu, T. L.; Nardi, K. L.; Draeger, N.; Hausmann, D. M.; Bent, S. F. Effect of Multilayer versus Monolayer Dodecanethiol on

Selectivity and Pattern Integrity in Area-Selective Atomic Layer Deposition, *ACS Appl. Mater. Interfaces* **2020**, *12*, 42226-42235.

(45) Greenwood, N. N.; Earnshaw, A., In *Chemistry of the Elements*, 2nd ed.; Butterworth-Heinemann: Oxford, 1998; p 522.

(46) Puurunen, R. L. Surface chemistry of atomic layer deposition: A case study for the trimethylaluminum/water process, *J. Appl. Phys.* **2005**, *97*, 121301.

(47) Puurunen, R. L.; Vandervorst, W. Island growth as a growth mode in atomic layer deposition: A phenomenological model, *J. Appl. Phys.* **2004**, *96*, 7686-7695.

(48) Some examples of ALD processes exhibiting substrate-enhanced growth are: (a) W ALD on $Al_2O_3$, (b) $Sb_2Se_3$ ALD on ZnS, (c) $Al_2O_3$ ALD on $Si_3N_4$, and (d) $TiO_2$ ALD on Ru (when $O_3$ is used as the co-reactant). See refs. 49-52.

(49) Wind, R. W.; Fabreguette, F. H.; Sechrist, Z. A.; George, S. M. Nucleation period, surface roughness, and oscillations in mass gain per cycle during W atomic layer deposition on $Al_2O_3$, *J. Appl. Phys.* **2009**, *105*, 074309.

(50) Mahuli, N.; Halder, D.; Paul, A.; Sarkar, S. K. Atomic Layer Deposition of an $Sb_2Se_3$ Photoabsorber Layer Using Selenium Dimethyldithiocarbamate as a New Se Precursor, *Chem. Mater.* **2019**, *31*, 7434-7442.

(51) Lamagna, L.; Wiemer, C.; Perego, M.; Spiga, S.; Rodríguez, J.; Coll, D. S.; Grillo, M. E.; Klejna, S.; Elliott, S. D. Mechanisms for Substrate-Enhanced Growth during the Early Stages of Atomic Layer Deposition of Alumina onto Silicon Nitride Surfaces, *Chem. Mater.* **2012**, *24*, 1080-1090.

(52) Lee, S. W.; Han, J. H.; Kim, S. K.; Han, S.; Lee, W.; Hwang, C. S. Role of Interfacial Reaction in Atomic Layer Deposition of $TiO_2$ Thin Films Using Ti(O-*i*Pr)$_2$(tmhd)$_2$ on Ru or $RuO_2$ Substrates, *Chem. Mater.* **2011**, *23*, 976-983.

(53) After the initial substrate has been covered, the different GPCs observed on H-Si and $SiO_2$/Si could perhaps be due to subtle differences in morphology or crystallinity at the surface of the growing antimony film. Similar phenomena have been reported for thermal or plasma-enhanced ALD of Ru, NiO and $TiO_2$. See refs. 54-56.

(54) Hwang, J. M.; Han, S. M.; Yang, H.; Yeo, S.; Lee, S. H.; Park, C. W.; Kim, G. H.; Park, B. K.; Byun, Y.; Eom, T.; Chung, T. M. Atomic layer deposition of a ruthenium thin film using a precursor with enhanced reactivity, *J. Mater. Chem. C* **2021**, *9*, 3820-3825.

(55) Song, S. J.; Lee, S. W.; Kim, G. H.; Seok, J. Y.; Yoon, K. J.; Yoon, J. H.; Hwang, C. S.; Gatineau, J.; Ko, C. Substrate Dependent Growth Behaviors of Plasma-Enhanced Atomic Layer Deposited Nickel Oxide Films for Resistive Switching Application, *Chem. Mater.* **2012**, *24*, 4675-4685.

(56) Won, S. J.; Suh, S.; Lee, S. W.; Choi, G. J.; Hwang, C. S.; Kim, H. J. Substrate Dependent Growth Rate of Plasma-Enhanced Atomic Layer Deposition of Titanium Oxide Using $N_2O$ Gas, *Electrochem. Solid-State Lett.* **2010**, *13*, G13-G16.

(57) At 95, 125 and 150 °C, pulse times of 1.0 or 2.0 s were also investigated for deposition on H-Si. At 95 °C, 1.0 and 2.0 s pulses led to slightly thicker films (after 1000 cycles, average film thickness values of 39 and 41 nm were obtained, respectively, vs 33 nm using 0.4 s pulses). The films now appeared visibly uniform, and VASE showed minimal variation in film thickness at different points on the wafer. By contrast, at 125 and 150 °C, 1.0s pulses still led to visibly patchy films, and VASE indicated substantial variations in film thickness at different points on the wafer.

(58) Use of an additional 20 minute argon purge between pre-treatment and the start of ALD was tested for (a) deposition on H-Si using $SbCl_3$ pre-treatment (50 x 0.8s pulses) prior to ALD (50 cycles using 0.8s pulses), and (b) deposition on $SiO_2$/Si using $Sb(SiMe_3)_3$ pre-treatment (50 x 0.4s pulses) prior to ALD (50 cycles using 0.4s pulses). The former yielded a film thickness of 6.5 nm (*cf.* 6.7 nm without the 20 minute argon purge), and the latter yielded a film thickness of 7.2 nm (*cf.* 7.1 nm without the 20 minute argon purge).

(59) Harris, R. K.; Becker, E. D.; De Menezes, S. M. C.; Goodfellow, R.; Granger, P. NMR nomenclature. Nuclear spin properties and conventions for chemical shifts - (IUPAC recommendations 2001), *Pure Appl. Chem.* **2001**, *73*, 1795-1818.

(60) Evans, C. M.; Castro, S. L.; Worman, J. J.; Raffaelle, R. P. Synthesis and use of tris(trimethylsilyl)antimony for the preparation of InSb quantum dots, *Chem. Mater.* **2008**, *20*, 5727-5730.

(61) Amberger, E.; Salazar G., R. W. Mixed Organometallic Compounds of Group V. I. Synthesis of Tris(trimethyl-group-IV)stibines, *J. Organomet. Chem.* **1967**, *8*, 111-114.

(62) von Hanisch, C. The Tris(triisopropylsilyl)pnikogenes: Synthesis and Characterization of E(Si$^i$Pr$_3$)$_3$ (E = P, As, Sb), *Z. Anorg. Allg. Chem.* **2001**, *627*, 1414-1416.

(63) Precursor bubblers (where argon flows through the bubbler during delivery, but does not actually bubble through the precursor; see Figure S29) rather than cylinders (which connect to the reactor via a single ALD valve) were used for all experiments. At room temperature (~23 °C), insufficient delivery was achieved when ALD was attempted with the precursors in cylinders, even with pulse durations of 10s.

(64) Eom, T.; Choi, S.; Choi, B. J.; Lee, M. H.; Gwon, T.; Rha, S. H.; Lee, W.; Kim, M.-S.; Xiao, M. C.; Buchanan, I.; Cho, D.-Y.; Hwang, C. S. Conformal Formation of $(GeTe_2)_{(1-x)}(Sb_2Te_3)_x$ Layers by Atomic Layer Deposition for Nanoscale Phase Change Memories, *Chem. Mater.* **2012**, *24*, 2099-2110.

(65) Knapas, K.; Hatanpää, T.; Ritala, M.; Leskelä, M. In Situ Reaction Mechanism Studies on Atomic Layer Deposition of $Sb_2Te_3$ and GeTe from $(Et_3Si)_2Te$ and Chlorides, *Chem. Mater.* **2010**, *22*, 1386-1391.

(66) Buriak, J. M. Organometallic chemistry on silicon and germanium surfaces, *Chem. Rev.* **2002**, *102*, 1271-1308.

(67) Jayachandran, S.; Delabie, A.; Billen, A.; Dekkers, H.; Douhard, B.; Conard, T.; Meersschaut, J.; Caymax, M.; Vandervorst, W.; Heyns, M. Deposition of O atomic layers on Si(100) substrates for epitaxial Si-O superlattices: investigation of the surface chemistry, *Appl. Surf. Sci.* **2015**, *324*, 251-257.

(68) Sun, Q. Y.; de Smet, L.; van Lagen, B.; Wright, A.; Zuilhof, H.; Sudholter, E. J. R. Covalently attached monolayers on hydrogen terminated Si(100): Extremely mild attachment by visible light, *Angew. Chem. Int. Ed.* **2004**, *43*, 1352-1355.

Authors are required to submit a graphic entry for the Table of Contents (TOC) that, in conjunction with the manuscript title, should give the reader a representative idea of one of the following: A key structure, reaction, equation, concept, or theorem, etc., that is discussed in the manuscript. Consult the journal's Instructions for Authors for TOC graphic specifications.